European Fate of Repository Gases Project: Preliminary numerical simulation of HG-A experiment in Mont-Terri with Code_Aster

FORGE Report D4.8– VER 1.0

	Name	Organisation	Signature	Date
Compiled	Fernandes Roméo / Granet Sylvie	EDF		
Verified				
Approved				

Keywords :

FORGE Experiment, Hydro-mechanical coupling, Drucker-Prager viscoplastic, Code_Aster numerical simulation.

Euratom 7th Framework Programme Project: FORGE

EURATOM

Fate of repository gases (FORGE)

The multiple barrier concept is the cornerstone of all proposed schemes for underground disposal of radioactive wastes. The concept invokes a series of barriers, both engineered and natural, between the waste and the surface. Achieving this concept is the primary objective of all disposal programmes, from site appraisal and characterisation to repository design and construction. However, the performance of the repository as a whole (waste, buffer, engineering disturbed zone, host rock), and in particular its gas transport properties, are still poorly understood. Issues still to be adequately examined that relate to understanding basic processes include: dilational versus visco-capillary flow mechanisms; long-term integrity of seals, in particular gas flow along contacts; role of the EDZ as a conduit for preferential flow; laboratory to field up-scaling. Understanding gas generation and migration is thus vital in the quantitative assessment of repositories and is the focus of the research in this integrated, multi-disciplinary project. The FORGE project is a pan-European project with links to international radioactive waste management organisations, regulators and academia, specifically designed to tackle the key research issues associated with the generation and movement of repository gasses. Of particular importance are the long-term performance of bentonite buffers, plastic clays, indurated mudrocks and crystalline formations. Further experimental data are required to reduce uncertainty relating to the quantitative treatment of gas in performance assessment. FORGE will address these issues through a series of laboratory and field-scale experiments, including the development of new methods for up-scaling allowing the optimisation of concepts through detailed scenario analysis. The FORGE partners are committed to training and CPD through a broad portfolio of training opportunities and initiatives which form a significant part of the project.

Further details on the FORGE project and its outcomes can be accessed at www.FORGEproject.org.

Contact details:

Author 1 Fernandes Roméo

Organisation EDF

EDF R&D

Analysis in Mechanics and Acoustics (AMA)

Tel: +33 (0)1.47.65.49.07 Fax +33 (0)1.47.65.41.18

email: romeo.fernandes@edf.fr

Address 1, avenue du Général de Gaulle – 92.140 Clamart – France.

Author 2 Granet Sylvie

Organisation EDF

EDF R&D

Analysis in Mechanics and Acoustics (AMA)

Tel: +33 (0)1.47.65.50.15 Fax +33 (0)1.47.65.41.18

email: sylvie.granet@edf.fr

Address 1, avenue du Général de Gaulle – 92.140 Clamart – France.

Contents

Figures

Summary

This report describes the firsts results obtained by EDF with the software Code_Aster in the simulation of the HG-A experiment on the Mont-Terri (Switzerland). In the first part of this report a brief presentation of the numerical software is given with a particular emphasize on the conceptual hydro-mechanical concepts. In the second part, a presentation of the HG-A experiment is done with a particular description of the hydraulical measurement obtained. And finally, in the third and last part, the results are presented and described taking into account the simplifications made to the simulations.

Introduction

The excavation of the underground works leads to the development of cracks and fractures in the rock that will modify the hydraulic properties of the soil creating preferred zones for gas and water flows. It appears essential to evaluate accurately the area of the excavation damaged zones around cylindrical excavations such as galleries, sealing sections in tunnels or shafts, and their evolution in porous media. This point is a crucial issue in the field of underground waste storage. In this goal, as part of a research programme in Mont-Terri HG-A, experiment has been started in 2005 and has been ended 4 years later (Marshall et al. 2006). The aim of this experience is the estimation of the extension of the damaged zone induced by the excavation works and it evolution due to the gas injection. The different main steps of this experience are :

- Micro-tunnel excavation in a overconsolidated claystone formation and site characterisation
- Backfill and seal emplacement
- Saturation phase
- Water injection
- Gas injection

This in-situ experiment is coupled with complementary laboratory program (two phase flow parameters, gas/water permeability). The rock formation was fully instrumented (Figure 1).

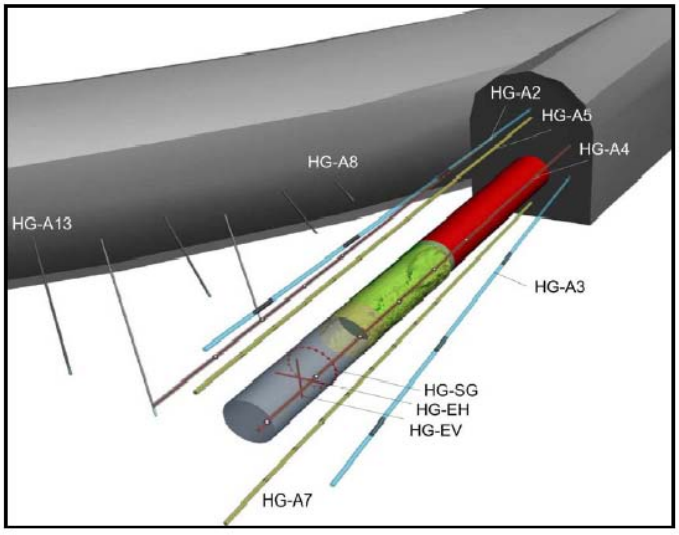

Figure 1 : Micro-tunnel with the three sections: liner (red), sealing (green), test (grey)

In this Workpackage, EDF will provide some numerical simulations using its finite element software Code_Aster. The first step of this work consists in HG-A experiment simulation with a focus on the Micro-tunnel excavation.

Description of numerical software Code_Aster and its conceptual models

Code_Aster [1] is a numerical software developed by EdF which offers a full range of multiphysical analysis and modelling methods that go well beyond the standard functions of thermomechanical calculation code. In particular, Code_Aster deals with thermo-hydro-mechanical problems with partial saturation in porous media, including the gas transfers. However, in this report, the thermal problem will not be considered and the medium will be considered fully saturated.

Hereafter are presented the general framework for saturated porous media and the conceptual model used for the modelling of the rock behaviour is emphasized.

1.1 GENERAL FRAMEWORK FOR SATURATED POROUS MEDIA

In this section, the balance equations for saturated porous media are firstly recalled. Then the constitutive equations of the mechanical and the fluid transfers problems are described. The complete description of the general framework for the modelling of the unsaturated case is presented in [2], [3], [4].

1.1. BALANCE EQUATIONS OF A POROUS VOLUME

In the numerical studies, the geomaterials of the geological layer are porous media generally considered as the superposition of several continua [5]: the solid skeleton (grains assembly) and the fluid phases (water, air, oil...). Based on averaging theories ([6] and [7]), [8] proposed the governing equations for the full dynamic behaviour of a partially saturated porous medium composed of three species (mineral, water and for example air) distributed in three phases (solid, liquid and gaseous phases). It is assumed that the mineral species and the solid phase coincide. However, the liquid phase may contain dissolved air and the gas phase is a mixture of dry air and water vapour.

Hereafter the balance equations are restricted for quasi-static problem in the water saturated case with isothermal conditions. The unknowns of the mechanical and the flow problems are respectively the displacements u_i, and the water pressure p_w. In the following developments, the balance equations are written in the current solid configuration (updated Lagrangian formulation).

2.1.1. Balance of momentum

In the mixture balance of momentum equation, the interaction forces between fluid phase and grain skeleton cancels. This equation reads:

$$div(\sigma)+(\rho_s(1-\varphi)+\rho_w\varphi)=0 \qquad (1)$$

where φ is the porosity, ρ_s is the solid grain density, ρ_w is the water density, σ is the total (Cauchy) stress tensor.

2.1.2. Solid mass balance equation

The balance equations are expressed in the moving current configuration through a Lagrangian actualised formulation. According to these assumptions, the mass balance equation of the solid skeleton is necessary met. For a given mixture volume *V*, the mass balance equation reads:

$$\frac{\partial \rho_s (1-\phi)\Omega}{\partial t} = 0 \qquad (2)$$

where *t* is the time and Ω is the volume of the porous medium.

2.1.3. Fluid mass balance equation

Following the ideas of Panday [9], the fluid mass balance equations are written for each chemical species (i.e. in our case : water). In this way the terms related to the phase transfer cancel. Hereafter the mass conservation equation for the water is presented :

$$\frac{\partial(\rho_w \varphi)}{\partial t} + div(\rho_w q_l) - Q_w = 0 \qquad (3)$$

where $\underline{q_l}$ is the advective flux of water (see next chapter for a detailed description of it) and Q_w is the sink term.

2.2. CONSTITUTIVE EQUATIONS

The constitutive equations are key components of the formulation. They describe the specific behaviour of the porous medium. Moreover the coupling phenomena are often reflected in the constitutive equations.

2.2.1. Stress-strain behaviour

In order to reproduce the stress-strain behaviour of totally saturated porous media, as the shear strength or the collapse phenomena, two separates stress variables are needed. Two main approaches exist. The first one is based on the net stresses and the second one is based on the Bishop's effective stress. For the simulation of this project we use the second one. Consequently we describe only the Bishop's effective stress in the particular case of saturated media:

$$\sigma'_{ij} = \sigma_{ij} - b p_w \delta_{ij} \qquad (4)$$

where σ' is the Bishop's effective stress, σ is the total stress, *b* is the Biot coefficient and p_w is the water pressure.

2.2.2. Solid density variation

For the considered materials and stress levels around radioactive waste disposals, the solid grain deformability is no more negligible and the general Biot framework [12] is used to model the hydromechanical coupled terms. Following the ideas of Biot, Coussy [13] proposed a thermodynamical framework of the problem, which leads to the expression of the porosity variation:

$$\dot{\varphi} = (b-\varphi)\left[\frac{\dot{p}_w}{K_s} + \dot{\varepsilon}_V\right] \qquad \text{with} \quad \dot{a} = \frac{\partial a}{\partial t} \qquad (5)$$

where $\dot{\varepsilon}_V$ is the skeleton volumetric deformation rate and K_s is the grain compressibility. The porosity variation is used in the fluid balance equations (eq. (3)) in the computation of the storage term. It introduces a coupling term between the mechanical behaviour and the fluid transfers.

2.2.3. Fluid transport constitutive equations

The advective flux of the water is governed by the Darcy's law:

$$q_l = -\frac{\underline{\underline{K}}_w}{\mu_w}\left(grad\left(p_w\right) + \rho_w g.grad(y)\right) \tag{6}$$

where $\underline{\underline{K}}_w$ is the water intrinsic permeability tensor, μ_w is the water dynamic viscosity, g the gravity acceleration and y the vertical upward directed coordinate.

2.2.4. Liquid density variation

The compressible fluid is assumed to respect the following relationship [8]. This predicts an increase of water density as a function of the water pressure, defining χ_w as the liquid water bulk modulus:

$$\dot{\rho}_w = \frac{\rho_w}{\chi_w}\dot{p}_w \tag{7}$$

2.2.5. Permeability variation

The permeability tensor $\underline{\underline{K}}_w$ can depend on the mechanical behaviour (porosity or tensile strain). For example, the permeability tensor can depend on porosity through Kozeny-Karman's law:

$$K = K_0\left(\frac{\varphi}{\varphi_0}\right)^3\left(\frac{1-\varphi_0}{1-\varphi}\right)^2 \tag{8}$$

where $\underline{\underline{K}}_0$ is the initial permeability, φ is the porosity and φ_0 is the initial porosity.

Other relationships take into account the coupling between permeability and porosity, as the one used in GDR Momas and initially proposed by Laigle [14]:

$$K = K_0\left(1 + \alpha\left(\varphi - \varphi_0\right)^{\beta}\right) \tag{9}$$

where α and β are material parameters.

2.2.6. Drücker-Prager Viscoplastic model – Mathematical formulation

In this section the mathematical formulation of the viscoplastic model based on Drücker Prager criterion developped in Code_Aster [15] is described. The proposed model is based on only one viscoplastic mechanism. The viscoplastic criterion hardening is due to the cumulated deviatoric plastic deformation, passing through three steps called thresholds: the initial threshold for a null viscoplastic deformation, the peak threshold for a peak deformation (parameter of the model) and a final threshold for a deformation beyond the ultim one (a parameter of the model). The stress state can be out of the threshold but it turns back with a speed proportional to the distance between the stress state and the threshold according to Perzyna law. The flow

is not associated, the flow potential is a Drucker-Prager one which hardens according to three levels (initial, peak, and ultim). Between the thresholds, hardening is linear.

In the following, *p* is the accumulated viscoplastic strain, S_{II} the second invariant of deviatoric stress tensor, I_1 the first invariant of stress, D_e the elastic tensor.

In this model, the yield surface is defined as :

$$f = \sqrt{\frac{3}{2}} S_{II} + \alpha(p) I_1 - R(p)$$

with, $\alpha(p)$, $R(p)$ function of p.

The viscoplastic potential G is defined by

$$G = \sqrt{\frac{3}{2}} S_{II} + \beta(p) I_1$$

To describe evolution of f and G, three levels are defined corresponding to three thresholds: the initial one matches the elastic part without viscoplastic deformation; the peak threshold characterizes the maximal stress state; and the final threshold corresponds to the residual state. Between the initial and the peak thresholds the behaviour is hardening. Between the peak and the residual thresholds the behaviour is softening. We note thereafter :

α_0, R_0, β_0 hardening parameters linked to elastic threshold $(p = 0)$

$\alpha_{pk}, R_{pk}, \beta_{pk}$ hardening parameters linked to peak threshold $(p = p_{pk})$

$\alpha_{ult}, R_{ult}, \beta_{ult}$ hardening parameters linked to final threshold $(p = p_{ult})$

Then, cohesion functions are defined as following:

$$\begin{cases} \alpha(p) = \left(\dfrac{\alpha_{pk} - \alpha_0}{p_{pk}} \right) p + \alpha_0 & \text{for} \quad 0 < p < p_{pk} \\ \alpha(p) = \left(\dfrac{\alpha_{ult} - \alpha_{pk}}{p_{ult} - p_{pk}} \right) (p - p_{pk}) + \alpha_{pk} & \text{for} \quad p_{pk} < p < p_{ult} \\ \alpha(p) = \alpha_{ult} & \text{for} \quad p > p_{ult} \end{cases}$$

the dilatancy functions are:

$$\begin{cases} \beta(p) = \left(\dfrac{\beta_{pk} - \beta_0}{p_{pk}} \right) p + \beta_0 & \text{for} \quad 0 < p < p_{pk} \\ \beta(p) = \left(\dfrac{\beta_{ult} - \beta_{pk}}{p_{ult} - p_{pk}} \right) (p - p_{pk}) + \beta_{pk} & \text{for} \quad p_{pk} < p < p_{ult} \\ \beta(p) = \beta_{ult} & \text{for} \quad p > p_{ult} \end{cases}$$

and the hardening functions:

$$\begin{cases} R(p) = \left(\dfrac{R_{pk} - R_0}{p_{pk}} \right) p + R_0 & \text{for} \quad 0 < p < p_{pk} \\ R(p) = \left(\dfrac{R_{ult} - R_{pk}}{p_{ult} - p_{pk}} \right) (p - p_{pk}) + R_{pk} & \text{for} \quad p_{pk} < p < p_{ult} \\ R(p) = R_{ult} & \text{for } p > p_{ult} \end{cases}$$

Stress and strains are linked with a classical Hooke's law: $\sigma = D_e \left(\varepsilon - \varepsilon^{vp} \right)$

The viscoplastic deformation is controled by the Perzyna law:

$$d\varepsilon_{ij}^{vp} = A \left\langle \frac{f}{p_{ref}} \right\rangle^n \frac{\partial G}{\partial \sigma_{ij}} dt$$

with p_{ref} the reference pressure (atmospheric pressure) and A creeping parameter.

EXCAVATION MODELING

Prior to the excavation, the rock was instrumented for monitoring the hydromechanical response to the drilling process. A complete description of the instrumentation of the rock with their responses is proposed by Marshall [16].

However, we just emphasize on some triple packer systems placed around the borehole. Their positions are described on Figure 3 : point A0 (named HG-A03) and point A1 (named HG-A02). We can notice that in 2D the triple packer is represented by a point. These packers are separated into three monitoring intervals labeled as "-i1" (12.5 - 14 m along hole), "-i2" (12 – 9.5 m ah) and "-i3" (9 - 5.5 m ah).

Figure 2(a) shows the evolution of pore pressure in the different monitoring intervals. In the short monitoring period before tunnel excavation, pore pressure in the observation intervals ranges between 0.75 and 0.9 MPa and increases slightly towards the expected (pseudo-)static formation pressure of about 1.0 – 1.2 MPa. Immediately after starting the tunnel excavation, a significant rise in pore pressure is seen in borehole BHG-A3, which is located at a distance of 0.5 m from the tunnel side wall.

Instantaneous failure of the rock was caused by the combined effect of the anisotropy in far-field stress, the anisotropy in geomechanical rock properties and the heterogeneity of the rock mass. We can see in

Figure 2(b) a scan of the HG-A micro-tunnel with the failure observed after the excavation. The breakouts occur on the upper left side (named position 9: 00 to 11: 00 o'clock).

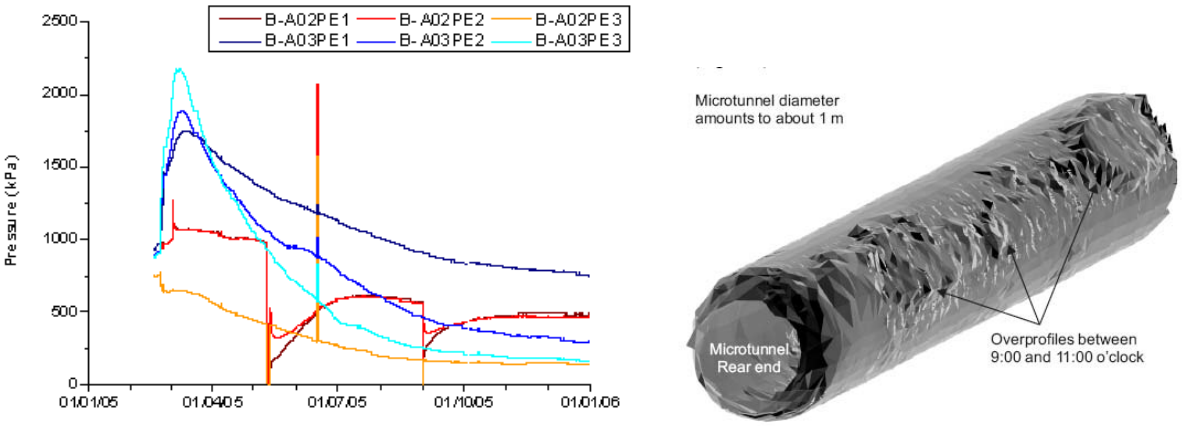

Figure 2: Experimental results. (a) on the left: The water pressure in triple packer HG-A02 and HG-A03. (b) on the right: 3D laser scan of the HG-A micro-tunnel with a tachymeter. Pictures extracted from Marshall et al [16].

NUMERICAL SIMULATION

The aim of this first simulation is to obtain results with a good agreement to the experimentation but considering the simplest modelisation. Consequently, in this framework we only simulate a 2D case (the geometry considered for the micro-tunnel is presented on Figure 3), without taking into account the geomechanical anisotropy of the medium.

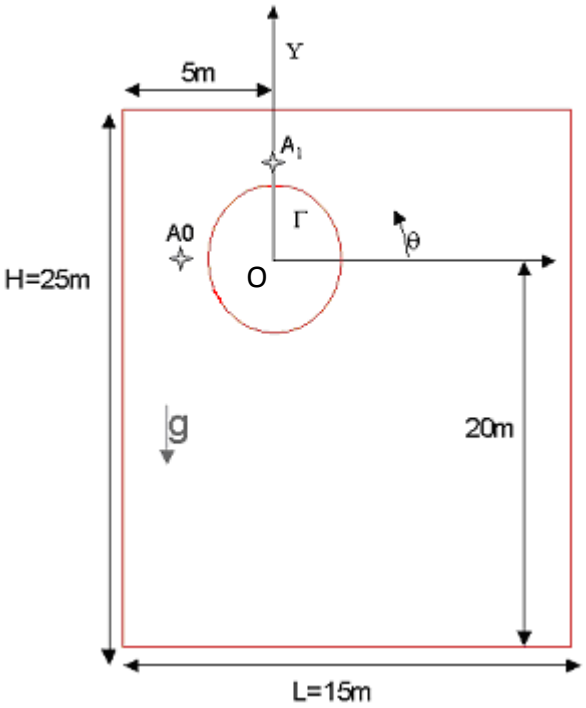

Figure 3 : Geometry of the micro-tunnel

The diameter of the micro-tunnel is about 1.036 meters and the dimensions of the box around it are about 15 meters following the horizontal axe and 25 meters following the vertical one. This particular conception of the geometry around the cavity is due to the in-situ proximity of other galleries.

The initial state of stress is anisotropic. In the horizontal axis in the center of the cavity (point O), the initial water pressure is about 0.8Mpa and the stresses are :

σ_Y^0 = 6,5Mpa (vertical direction)

σ_Z^0 = 2,5Mpa (NE-SW direction)

σ_X^0 = 4,5Mpa (NW-SE direction)

Taking into account the gravity, the initial water pressure and the stresses in the modelisation are defined by a function of the gravity acceleration g:

$p_w = -\rho_w g Y + 0.8MPa$ (where Y=0 is the center of the cavity)

$\sigma_\lambda = -\rho_s g Y + \sigma_\lambda^0$ (where $\lambda = x, y, z$)

For the excavation experimentation, the duration of the works is about 7 days for a 13 meters long cavity, and the measurement of the hydraulical pressure evolution will continue 11 monthes (we call this last step the consolidation phase). For the simulation we only consider a bidimensionnal test and consequently we take into account an excavation phase of one day with the convergence-confinement methodology (a complete description of this methodology is presented in [18]).

The mechanical behaviour of the rock that we consider is a simple Drucker-Prager viscoplastic model which is described in the previous section. The parameters used are the following ones:

$$E_{young} = 2760MPa; \qquad \nu = 0.27$$

$$\alpha_0 = 0.0001; \qquad \alpha_{pic} = 0.5; \qquad \alpha_{ult} = 0.4$$

$$\beta_0 = -0.01; \qquad \beta_{pic} = -0.1; \qquad \beta_{ult} = 0.1$$

$$R_0 = 1.54e6; \qquad R_{pic} = 2.9e6; \qquad R_{ult} = 0.9e6$$

$$A = 1.5e{-}11; \qquad n = 4$$

$$p_{pic} = 0.0039; \qquad p_{ult} = 0.0055$$

These parameters are identified in order to fit the experimental results presented by Laloui and François [17] in a triaxial compression test with a confinement of 5 Mpa. Figure 4(a) shows the equivalent deviatoric stresses of a biaxial simulation which take into account an initial isotropic stress state and the previous parameters. In the Figure 4(b) is plotted the evolution of the associated volumetric strain.

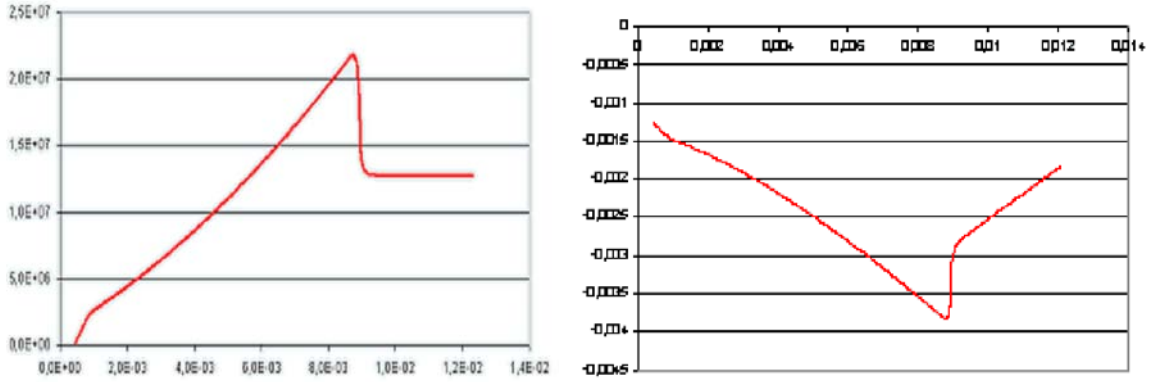

Axial strains

Axial strains

Figure 4 : (a) on the left: deviatoric stresses in Pa, and (b) on the right: volumic strains

To complete the modelisation the following parameters are used for the hydraulical part :

$\varphi_0 = 0.156$	initial porosity
$b = 0.76$	Biot coefficient
$\rho_w = 1000\, kg/m^3$	water density
$\mu_w = 0.001\, Pa.s$	water dynamic viscosity
$\chi_w = 2000\, MPa$	water bulk modulus
$K_w = 1.0e^{-19}\ m^2$	water intrinsic permeability
$\rho_s = 2450\, kg/m^3$	solid grain density

RESULTS

In Figure 5 we present the evolution of the water pressure obtained with Code_Aster at the point A0 (see Figure 3) along the HG-A3 triple packer system during 25 weeks after the excavation process. To reproduce the non-classical increase of water pressure after the excavation phase we should consider a rock with a great contractancy (as reproduced in Figure 4b). Indeed, such phenomenon induced a reduction of the pore volume which instantaneously generate an increase of the water pressure.

The results obtain in this simulation are satisfying. Indeed, the water pressure curve is in good agreement with the experimental ones taking into account that we consider a bidimensional isotropic problem to reproduce a tridimensional anisotropic phenomenology.

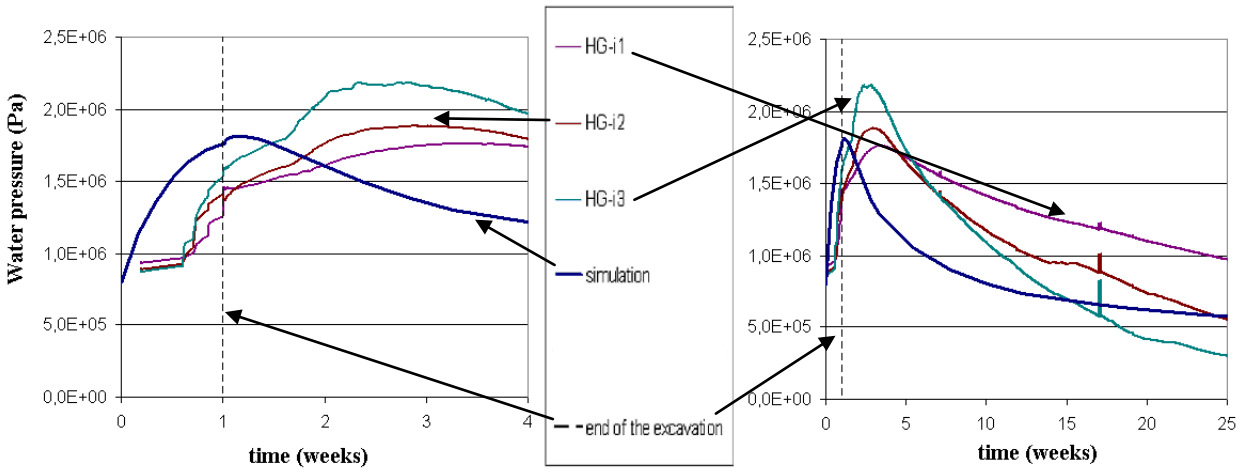

Figure 5 : Water pressure along HG-A3 triple packer system

In Figure 6, we present the water pressure evolution at the point A1 (see Figure 3). We can notice that at this point the water pressure decrease during the excavation phase as the experimental measurement of the packer HG-i3. However, we notice on the same experimental measurement some peaks of water pressure (weeks 17 / 12 and 28). We don't know exactly the phenomenology produced at these times : some water injection, an error of the measurement or whatelse? Consequently we don't reproduce them in our simulation. We can observe that this unknown phenomenology modifie also the measurement on the other packers (respectively HG-i1 and HG-i2). Indeed we can notice a progressive increase of the water pressure measurement on the two last packers which can suppose that is not an error of measurement in the packer HG-i3.

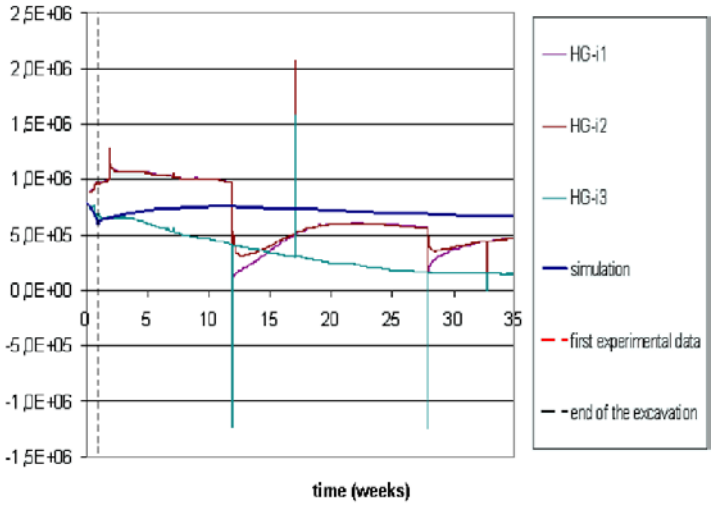

Figure 6 : Water pressure along HG-A2 triple packer system

To complete the hydraulical analysis we can observe on Figure 7 the repartition of the water pressure on the structure at the end of the excavation and after 25 weeks of consolidation. We can notice a strong increase of the water pressure near the horizontal plane of the cavity due to the contractancy evolution on the media (this point will be observed on the Figure 8 which presents the mechanical phenomenology).

In the vertical plane near the cavity we observe a decrease of the water pressure which can be explained by the boundary conditions on the cavity. This decrease is simply due to the water

flows. After the consolidation phase we can observe a redistribution of the water pressure on the structure. Around the cavity we can notice an homogeneous variation of the water pressure due to the boundary condition (water pressure imposed to simulate the ventilation of the gallery). On the top of the structure we also notice the effect of the boundary condition (water pressure imposed) but this one doesn't have any impact on the points of observation A0 and A1.

In the Figure 8 we can notice a classical ovalisation of the deformation around the cavity due to the anisotropic initial state of stress of the medium. However, we don't observe a degradation between 9:00 to 11:00 o'clock as in

Figure 2 due to the non-consideration in our modelisation of the anisotropic behaviour.

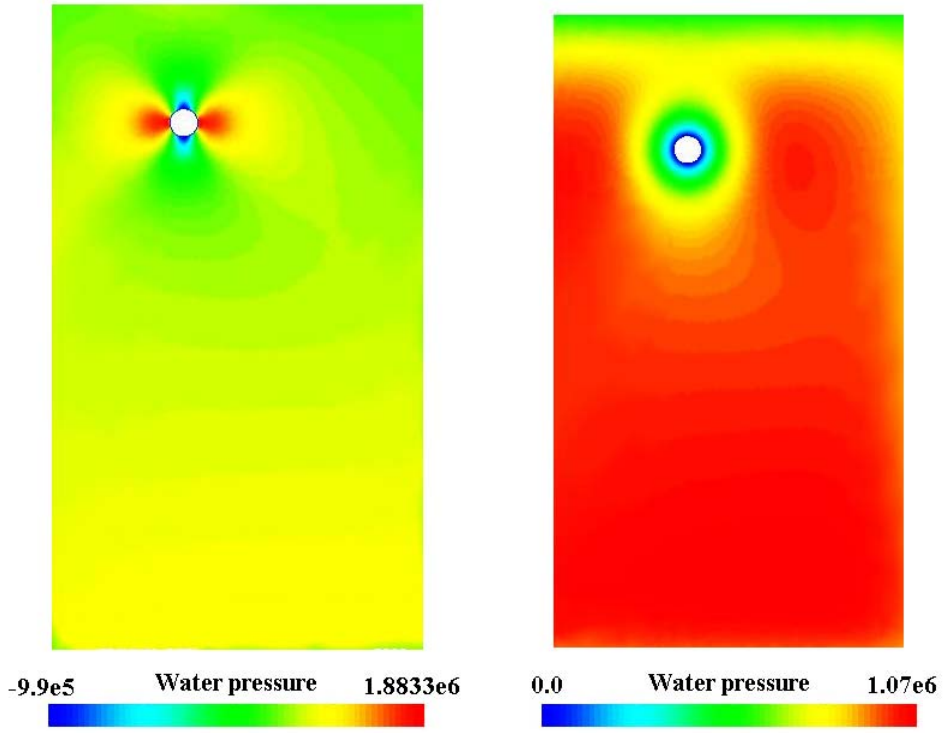

Figure 7 : Isovalues of water pressure after the excavation (on the left) and after 25 weeks of consolidation (on the right)

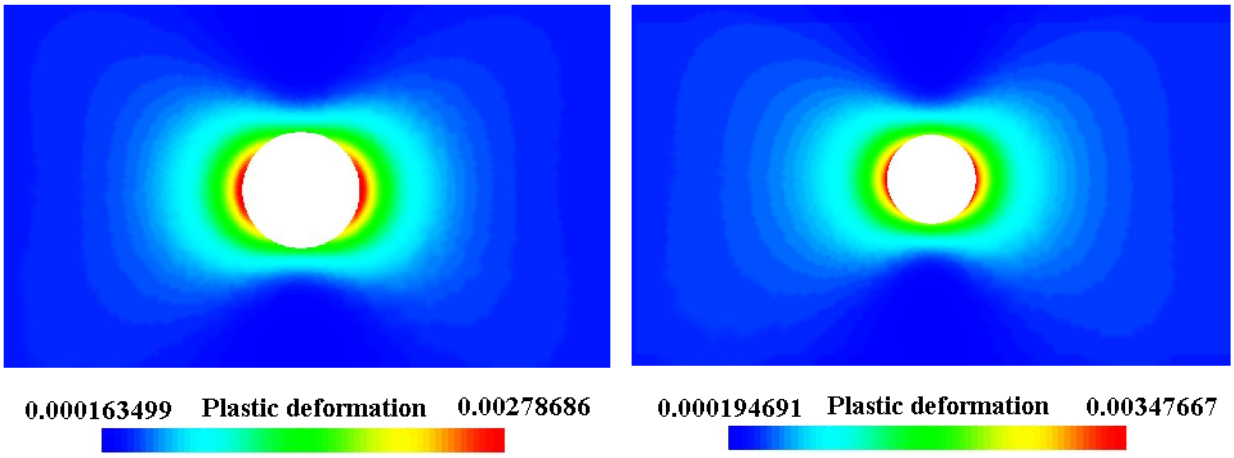

Figure 8 : Isovalues of the plastic deformation after the excavation (at left) and after 25 weeks of consolidation (at right)

Conclusion and Perspectives

In this report we present the first results obtained in the simulation of the HGA-excavation and consolidation at Mont-Terri in the scope of the European Forge Project. The hydro-mechanical simulations are produced with the software Code_Aster of EDF.

The results obtained are satisfying taking into account the hypothesis simplification of the simulation : water saturated medium, isotropic hydro-mechanical behaviour, bidimensional analysis. Indeed, the numerical results are quite in good agreement with the experimental measurement.

In order to obtain a better fit of the experimental measurement, some numerical simulations will be done with a new set of datas. Among them we can emphasize on :

- The hydraulical anisotropic behaviour;
- The mechanical anisotropic behaviour;
- The evolution of the permeability in the damaged zone;
- The complete 3D simulation;
- Finally, we will take into account the unsaturated conditions in order to modelize the gaz injection (second step of the project).

References

[1] Code_Aster, **www.code-aster.org**.

[2] P.Gerard, R.Charlier, F.Collin, R.Fernandes, S.Granet, D.Arnedo, S.Olivella, Description of initial numerical codes and conceptual model (undisturbed and disturbed host rocks). Forge Project – Deliverables 4.5 and 5.5 (February 2010).

[3] S. Granet, Modélisations THHM : Généralités et algorithms, doc R7.01.10, available on **www.code-aster.org**.

[4] S. Granet, Modèles de comportement THHM, doc R7.01.11, available on **www.code-aster.org**.

[5] Coussy O. 1995. *Mechanics of Porous Continua*. Wiley, London.

[6] Hassanizadeh M., Gray W. 1979. General conservation equations for multi-phase systems: 1. Average procedure. *Advances in Water Resources*. **2**, 131–144.

[7] Hassanizadeh M., Gray W. 1979. General conservation equations for multi-phase systems: 2. Mass, momenta, energy, and entropy equations. *Advances in Water Resources*. **2**, 191–208.

[8] Lewis RW., Schrefler B.A. 2000. *The Finite Element Method in the Static and Dynamic Deformation and Consolidation of Porous Media*. Wiley, New York.

[9] Panday S., Corapcioglu M.Y. 1957. Reservoir transport equations by compositional approach. *Transport in Porous Media*. **4,** 369-393.

[10] Olivella S., Carrera J., Gens A., Alonso E.E. 1994. Nonisothermal multiphase flow of brine and gas through saline media. *Transport in Porous Media*. **15**, 271-293.

[11] Nuth M., Laloui L. 2008. Effective stress concept in unsaturated soils: Clarification and validation of a unified framework. *International Journal for Numerical and Analytical Method in Geomechanics*. **32**, 771–801.

[12] Biot M.A. 1941. General theory of three-dimensional consolidation. *Journal of Applied Physics*. **12**, 155-164.

[13] Coussy O. 2004. *Poromechanics*. Wiley, London.

[14] F.Laigle, Modèle conceptuel pour le développement de lois de comportement adaptées à la conception des ouvrages souterrains. Thèse de Doctorat, Ecole Centrale de Lyon.

[15] R.Fernandes, Loi de comportement viscoplastique VISC_DRUC_PRAG. doc R7.01.22, available on **www.code-aster.org**.

[16] Marshall, P. & Distinguin, M. & Shao, H. & Bossart, P. & Enachescu, C. & Trick, T. (2006). Creation and Evolution of Damage Zones Around a Microtunnel in a Claystone Formation of the Swiss Jura Mountains. SPE-98537-PP.

[17] L.Laloui, B.François, Benchmark on Constitutive Modelling of the Mechanical Behaviour of Opalinus Clay EPFL report.

[18] P.Mestat et al, Ouvrages en interaction, HERMES Science Publications, 1999.